Doxorubicin@Bcl-2 siRNA core@shell nanoparticles for synergistic anticancer chemotherapy

ACS APPLIED BIO MATERIALS

Article

Doxorubicin@Bcl-2 siRNA core@shell nanoparticles for synergistic anticancer chemotherapy

Mengjiao Zhou, Xiujuan Zhang, Xiuzhen Xu, Xianfeng Chen, and Xiaohong Zhang

ACS Appl. Bio Mater., **Just Accepted Manuscript** • Publication Date (Web): 05 Jul 2018

ACS Publications

is published by the American Chemical Society. 1155 Sixteenth Street N.W., Washington, DC 20036

Doxorubicin@Bcl-2 siRNA core@shell nanoparticles for synergistic anticancer chemotherapy

Mengjiao Zhou,[+] *Xiujuan Zhang,*[+,*] *Xiuzhen Xu,*[+] *Xianfeng Chen,*[‡,*] *and Xiaohong Zhang*[+,*]

+Jiangsu Key Laboratory for Carbon-Based Functional Materials & Devices, Institute of Functional Nano & Soft Materials (FUNSOM), Joint International Research Laboratory of Carbon-Based Functional Materials and Devices, Soochow University, 199 Ren'ai Road, Suzhou, 215123, Jiangsu, PR China.

‡School of Engineering, Institute for Bioengineering, The University of Edinburgh, King's Buildings, Mayfield Road, Edinburgh EH9 3JL, United Kingdom.

Abstract

Acquired drug resistance in malignant tumors seriously hinders effective chemotherapy against cancer. The main mechanisms of drug resistance include decreased drug influx, increased drug efflux, as well as anti-apoptotic defense behavior in cancerous cells. To overcome these issues, we design a nanomedicine composed of pure doxorubicin (DOX) as the core and B-cell lymphoma-2 (Bcl-2) siRNA as the shell for synergistic cancer treatment. Between the core and shell, polyethylene glycol (PEG) and polyethylenimine (PEI) are employed to increase the stability of the core DOX NPs and

facilitate siRNA coating, respectively. In this design, the siRNA is able to inhibit the expression of Bcl-2 protein which has a role of protecting cancer cells from apoptosis. DOX is not only for anticancer therapy, but also acts as a nanocarrier for Bcl-2 siRNA delivery. Our studies show that Bcl-2 siRNA and DOX are efficiently delivered into tumor cells and tumor tissues, and such a co-delivery nanosystem possesses synergistic effects on tumor inhibition, enabling significantly enhanced anti-tumor outcome. This work demonstrates that the co-delivery of tumor suppressive Bcl-2 siRNA and chemotherapeutic agents without using an excipient material as a drug carrier represents a promising therapy for enhanced cancer therapy.

Keywords: drug resistance; Bcl-2 siRNA; doxorubicin; co-delivery nanosystem; synergistic efficacy

1. Introduction

Multidrug resistance (MDR) of cancerous cells is one key factor that limits the effectiveness of current chemotherapy for tumor treatment.[1,2] The main mechanisms of MDR include decreased drug influx, increased drug efflux, as well as anti-apoptotic defense behavior in cancerous cells.[3,4] For example, B-cell lymphoma-2 (Bcl-2) is a well-known anti-apoptotic protein which situates at the outer mitochondrial membrane and can prevent apoptosis-inducing factor to enter cytoplasm and thereby inhibit cancer cell apoptosis.[5,6] To avoid cancer cells being protected from apoptosis, it is apparent that Bcl-2 targeted siRNA can be employed to inhibit the expression of Bcl-2 protein.[7,8] However, there are many obstacles for efficient transport and transfection of siRNA such as intense negative charge, large molecular weight, and enzymatic degradation in

endosomes and lysosomes.[9,10] To address these problems, various nanocarriers including polymeric, liposomal, and silica-based cationic nanoparticles (NPs) have been reported for siRNA delivery.[11-13] However, these techniques possess a low drug loading capacity of generally below 30%.[14-16] More importantly, these nanocarriers themselves do not play any therapeutic role and a large amount may be accumulated in patients over a long period of treatment, which will ultimately cause serious toxicity and inflammation.[17-19]

For enhanced drug delivery systems, we design to employ pure anticancer drug molecules to synthesize NPs and then use them as a carrier to deliver siRNA gene for synergistic therapy. In this approach, the nanocarrier is made of pure drug molecules with a therapeutic role and will therefore alleviate the problem of introducing a large dose of excipient material during cancer treatment.[20,21] In addition, combined therapy containing multiple antitumor agents is a highly effective strategy to treat cancers, especially those with acquired drug resistance.[22-24] In such combinatorial treatment, simultaneous use of chemotherapeutic drug molecules and genetic components is particularly efficient in improving anticancer effect compared with individual therapy.[25,26] The main reasons are that chemotherapeutic drugs induce apoptotic cell death,[27,28] and, in the meantime, genes and genetic elements can increase the sensitivity of cells to chemotherapeutic drugs.[29,30]

With this strategy, we herein report a Bcl-2 siRNA capped doxorubicin NPs (DOX@siRNA core@shell NPs) to realize a combinatorial therapy for enhanced anticancer efficacy (**Scheme 1**). Apparently, beyond therapeutic function, DOX NPs

also play a role as a nanocarrier for siRNA delivery. In this work, we synthesized DOX@siRNA NPs and then systematically investigated the morphology, size, and biocompatibility of the nanomedicine as well as its *in vitro* intracellular delivery and *in vivo* therapeutic efficacy.

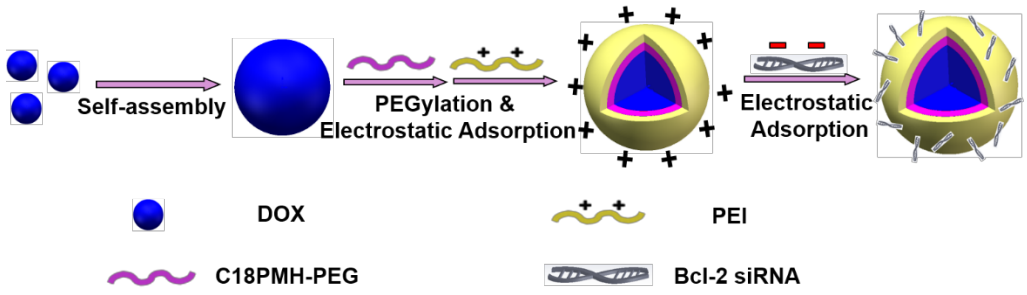

Scheme 1. The construction of DOX@siRNA NPs.

2. Results and discussion

2.1. Preparation and characterization of DOX@siRNA NPs

The preparation of DOX@siRNA NPs involves the following steps. First, hydrophobic DOX is prepared by removal of hydrochloric acid from as-purchased hydrophilic DOX under alkaline conditions. Second, DOX NPs are produced using a solvent exchange method (**Figure 1a**). The diameter of these NPs is about 52 nm and the zeta potential is -17.2±0.41 mV (**Figure 1c** and **d**), as determined by a Zetasizer Nano ZS (Malvern Instruments). To improve the bio-stability and long-circulating ability of DOX NPs in blood stream, amphiphilic C18PMH-PEG copolymer molecules are applied to modify the particles' surface in the third step (Figure S1).[31] With PEG coating, the size of the DOX-PEG NPs slightly increases to about 53 nm and the zeta potential remains negative charged (–14.2±1.19 mV, **Figure 1c** and **d**). Fourth, positive

charged PEI is adsorbed to the surface of PEG tailored NPs through electrostatic attraction (DOX-PEG-PEI NPs) and render the surface positive charge (+22.3±1.21 mV, **Figure 1d**). The size of the NPs further increases to about 55 nm (**Figure 1c**). Finally, negatively charged Bcl-2 siRNA is attached to the PEI modified surface again through electrostatic attraction to form the outmost shell of the NPs (DOX@siRNA NPs, **Figure 1b**).

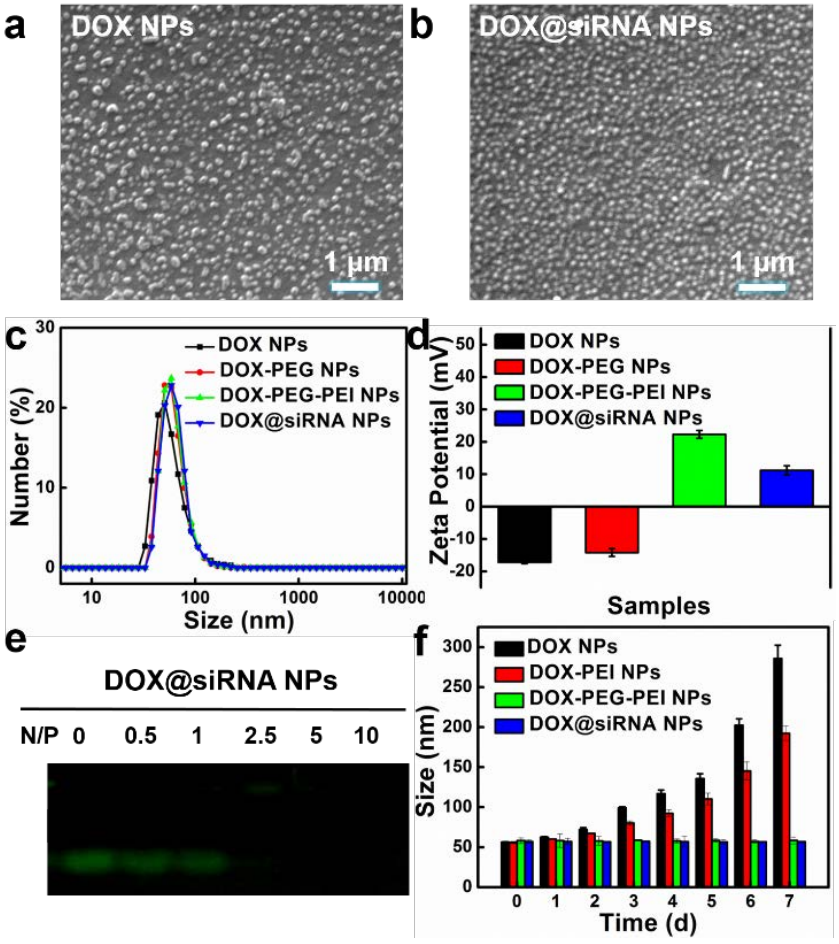

Figure 1. Characteristics of DOX@siRNA NPs. Scanning electron microscopy (SEM) images of (a) DOX NPs and (b) DOX@siRNA NPs (FEI Quanta 200). (c) Size and (d) Zeta potentials of DOX NPs, DOX-PEG NPs, DOX-PEG-PEI NPs and DOX@siRNA NPs. (e) Electrophoretic mobility of siRNA loaded DOX@siRNA NPs at different N/P

ratios. (f) Seven days stability studies of samples in PBS.

To explore the condition under which siRNA molecules are firmly loaded onto the surface of PEI modified NPs, various N/P ratios (0.5, 1, 2.5, 5, and 10) between the combination of PEI modified NPs and Bcl-2 siRNA were tested and the influence of the ratio on the mobility of siRNA was investigated by gel retardation assay using pure siRNA as a control. If siRNA molecules tightly bind to NPs, they will not move in the gel. As displayed in **Figure 1e**, strong binding of siRNA on NPs can be achieved when the N/P ratio is 5/1 or greater. This is indicated by the fact that siRNA does not move in the gel at this ratio. Therefore, in this work, DOX@siRNA NPs were produced at N/P ratio of 5/1. At this ratio, with the loading of siRNA, the zeta potential of the NPs decreases to 10.2±0.89 mV. The drug payload of DOX@siRNA NPs could reach as high as 87.18%, which is significantly higher than carriers-based nanomedicines.

The stability of DOX NPs, DOX-PEI NPs, DOX-PEG-PEI NPs, and DOX@siRNA NPs was investigated by measuring their sizes in PBS over a period of 7 days. As shown in **Figure 1f**, DOX NPs and DOX-PEI NPs without surface PEGylation experience a rapid size growth and quickly form large agglomerations in PBS. In contrast, DOX-PEG-PEI NPs exhibit a high stability in PBS over the 7 days observation period, demonstrating the necessity of NPs surface modification with C18PMH-PEG polymer. After loading of siRNA on the surface, the obtained DOX@siRNA NPs can also maintain stable size with negligible size increase, making it possible for drug delivery in biological environment.

2.2. *In vitro* release activity of DOX@siRNA NPs

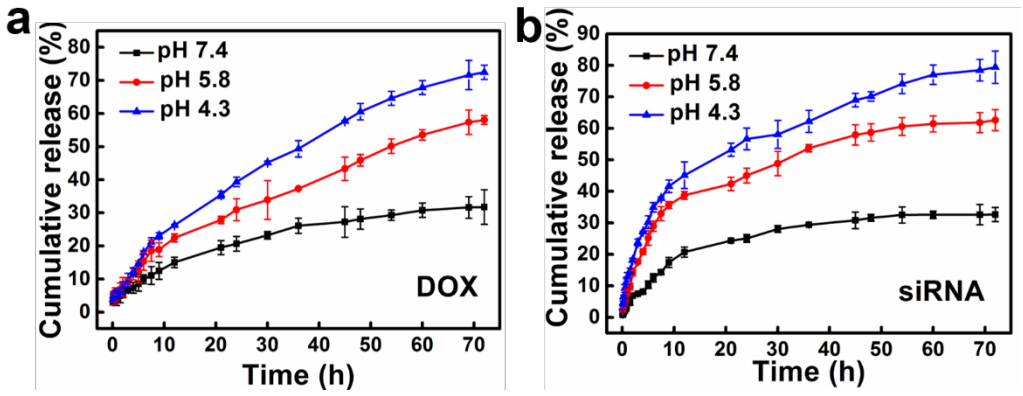

Figure 2. The release profiles of DOX@siRNA NPs. The release amount of (a) DOX and (b) siRNA at different pH values of 7.4, 5.8, and 4.3.

In order to study the release of DOX and siRNA, DOX@siRNA NPs were placed in three buffer solutions with different pH values including 7.4, 5.8, and 4.3 for a duration of 72 hours. These three pH values were selected to simulate the acidity and alkalinity of bloodstream transportation (pH 7.4) and lysosome (pH between 4.3 and 5.8). The release of DOX and fluorescein-labeled siRNA (FAM-siRNA) was collected through dialysis and the amount was monitored by measuring their fluorescence. It can be seen that in **Figure 2a**, at pH 7.4, 20.64% and 31.73% of DOX is released from DOX@siRNA NPs at 24 and 72 h, respectively. In comparison, the increase of acidity can significantly improve the release rate of DOX. At pH 5.8, 30.94% and 58.04% of DOX is liberated from NPs at 24 and 72 h, respectively. The release becomes more drastic at pH 4.3 at which 39.33% and 72.43% of DOX liberates from NPs at 24 and 72 h, respectively. Similar results are also shown for the release profiles of siRNA at different pH values (**Figure 2b**). These phenomena indicate that DOX@siRNA NPs can release the incorporated drugs more rapidly in the acidic tumor environment,

thereby enhancing their anticancer efficacy.

2.3. *In vitro* therapeutic activity of DOX@siRNA NPs

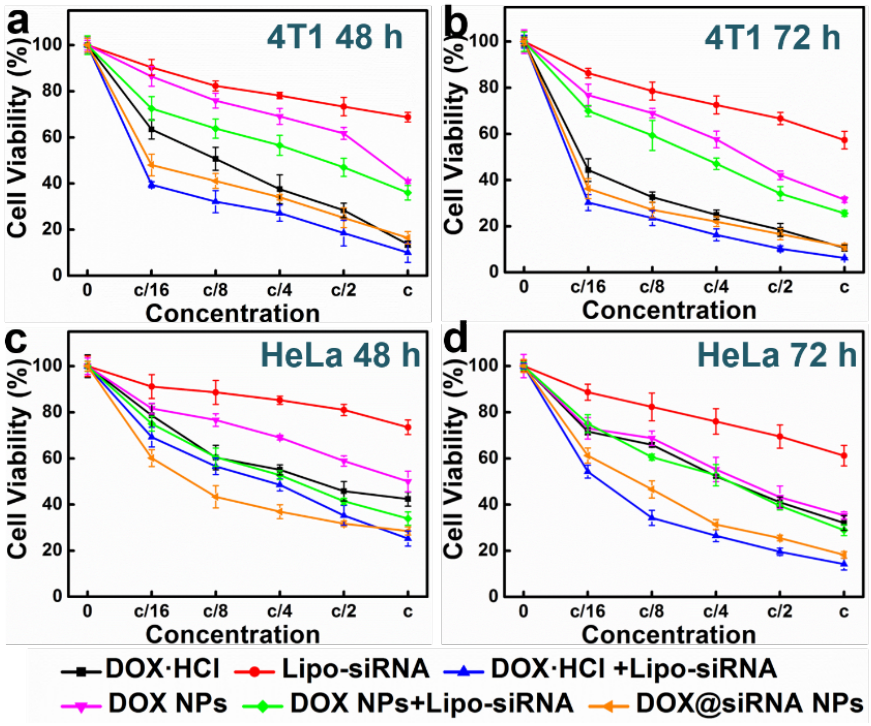

Figure 3. *In vitro* cytotoxicities of DOX@siRNA NPs against normal cancerous cells. Cell viabilities of 4T1 cells (a, b) and HeLa cells (c, d) when incubated with (1) DOX•HCl, (2) Lipo-siRNA, (3) DOX•HCl plus Lipo-siRNA, (4) DOX NPs, (5) DOX NPs plus Lipo-siRNA, and (6) DOX@siRNA NPs for 48 and 72 h. The highest concentrations, c, respectively represented (1) 20 μg/mL DOX, (2) 50 nM siRNA, (3) 10 μg/mL DOX /25 nM siRNA, (4) 20 μg/mL DOX, (5) 10 μg/mL DOX/25 nM siRNA, and (6) 10 μg/mL DOX/25 nM siRNA.

Our characterizations show that DOX@siRNA NPs have high stability, preferred release profiles for anticancer therapy, and desirable size for drug delivery. To assess their therapeutic efficacy, we firstly investigated the anti-proliferative effect using a

MTT assay against 4T1 cancer cells and HeLa cancer cells. For proving DOX@siRNA NPs' synergistic effect in anticancer treatment, the cytotoxicities of DOX•HCl, lipofectamine loaded Bcl-2 siRNA (Lipo-siRNA), DOX•HCl plus Lipo-siRNA, DOX NPs, and DOX NPs plus Lipo-siRNA (simple physical mixture of the two) were also measured for comparison. As indicated in **Figure 3a**, with the highest concentration and at 48 hours after drug application, DOX•HCl plus Lipo-siRNA (10.02% viability) exhibit a slightly higher anti-proliferative effect in comparison with individual DOX•HCl (13.66% viability) and Lipo-siRNA (69.72% viability). Moreover, DOX NPs plus Lipo-siRNA (35.99% viability) exhibited a higher anti-proliferative effect in comparison with DOX NPs (47.68% viability) and Lipo-siRNA (69.72% viability). These results indicate that the combination of DOX and Bcl-2 siRNA possesses synergetic effect. Attractively, DOX@siRNA NPs display a significantly higher anti-proliferative effect (13.66% viability) than the simple physical mixture of DOX NPs and Lipo-siRNA group (40.90% viability). This may be due to the fact that DOX@siRNA NPs aid the delivery of siRNA, enabling the simultaneous transport of both therapeutics to the treated cells. By 72 h after incubation (**Figure 3b)**, DOX@siRNA NPs possess a moderately increased efficacy of 10.61% viability, demonstrating the effectiveness in killing cancer cells. Furthermore, the combination index (CI) analysis was calculated by evaluating the anticancer efficacy of DOX NPs, Lipo-siRNA and DOX@siRNA NPs against HeLa cells. The CI values of below 1 represents synergism. In our experiments, all CI values of DOX@siRNA NPs are obviously below 1, indicating the synergistic antitumor effect of DOX and Bcl-2 siRNA

in our DOX@siRNA NPs design. Similar results are observed in the case of treating HeLa cells with these drugs as shown in **Figure 3c** and **d**. These anti-proliferative effect assays prove an excellent potential of utilizing DOX@siRNA NPs for efficient synergistic therapy.

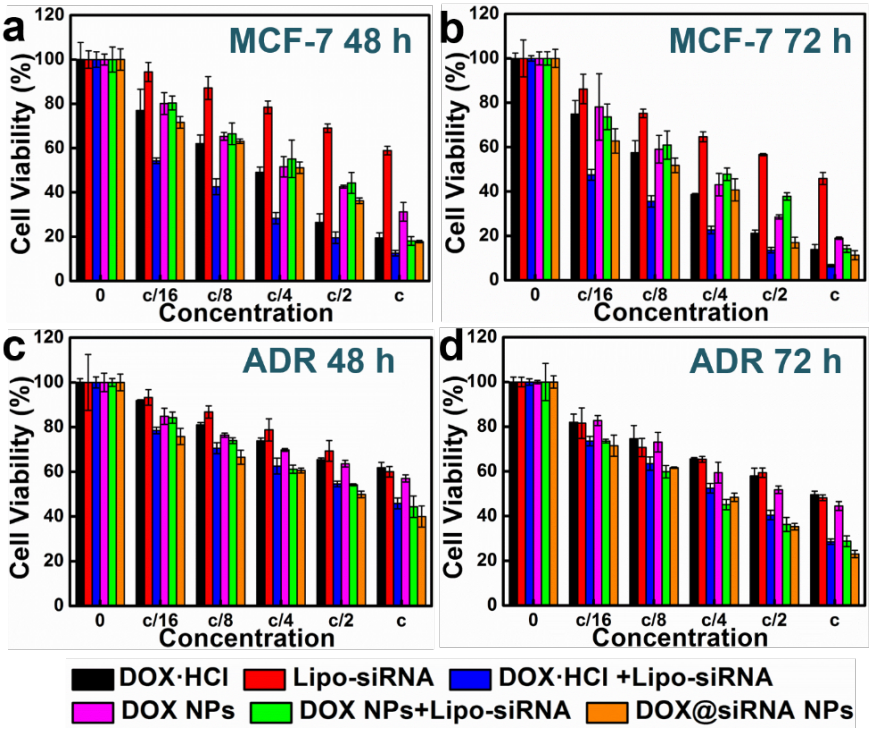

Figure 4. *In vitro* cytotoxicities of DOX@siRNA NPs against drug resistant cancer cells. Cell viabilities of (a, b) MCF-7 cells and (c, d) MCF-7/ADR cells when incubated with (1) DOX•HCl, (2) Lipo-siRNA, (3) DOX•HCl plus Lipo-siRNA, (4) DOX NPs, (5) DOX NPs plus Lipo-siRNA, and (6) DOX@siRNA NPs for 48 and 72 h, respectively. The concentrations were as the same as the above MTT experiments.

Following the confirmation that DOX@siRNA NPs can effectively kill normal cancer cells, we next studied whether the material is able to overcome drug resistant ones. For this purpose, we treated MCF-7/ADR cells, a DOX resistant derivatives of MCF-7 cells which overexpressing Bcl-2, with our DOX@siRNA NPs. DOX•HCl,

Lipo-siRNA, DOX•HCl plus Lipo-siRNA, DOX NPs and DOX NPs plus Lipo-siRNA were set as control groups. The results are presented in **Figure 4**. Firstly, although DOX•HCl show potent efficacy in killing normal MCF-7 cells (13.80% viability at the highest drug concentration after 72 h incubation), the function is much less effective for MCF-7/ADR cells (49.54% viability under the same condition). The reduction of efficacy is even more obvious with shorter period of incubation such as 48 h. For example, the viability of MCF-7/ADR cells remains above 60% at 20 μg/mL DOX•HCl after 48 h. Similar phenomenon also occurs on DOX NPs. Again, at the highest concentration, the viabilities of MCF-7 cells and MCF-7/ADR cells are 18.56% and 44.52%, respectively, after incubation with DOX NPs for 72 h. The over expression of Bcl-2 on MCF-7/ADR cells might be an important reason for drug resistance.[32,33] The combinatorial therapy of physical mixture of DOX and Bcl-2 siRNA (DOX•HCl plus Lipo-siRNA, DOX NPs plus Lipo-siRNA) can alleviate the drug resistance of cancer cells.[34,35] This is reflected from the result of low viability of drug resistant cells when incubated with DOX•HCl plus Lipo-siRNA (28.55%), and DOX NPs plus Lipo-siRNA (28.78%) after 72 h incubation. These values are dramatically lower than the viabilities of 49.54% and 44.52% for the groups of DOX•HCl and DOX NPs, respectively. Moreover, DOX@siRNA NPs can further enhance the efficacy against drug resistant cancer cells to the viability of 23.06%, revealing a greaet potential with respect to MDR reversal in chemotherapy.

2.4. Intracellular uptake of DOX@siRNA NPs

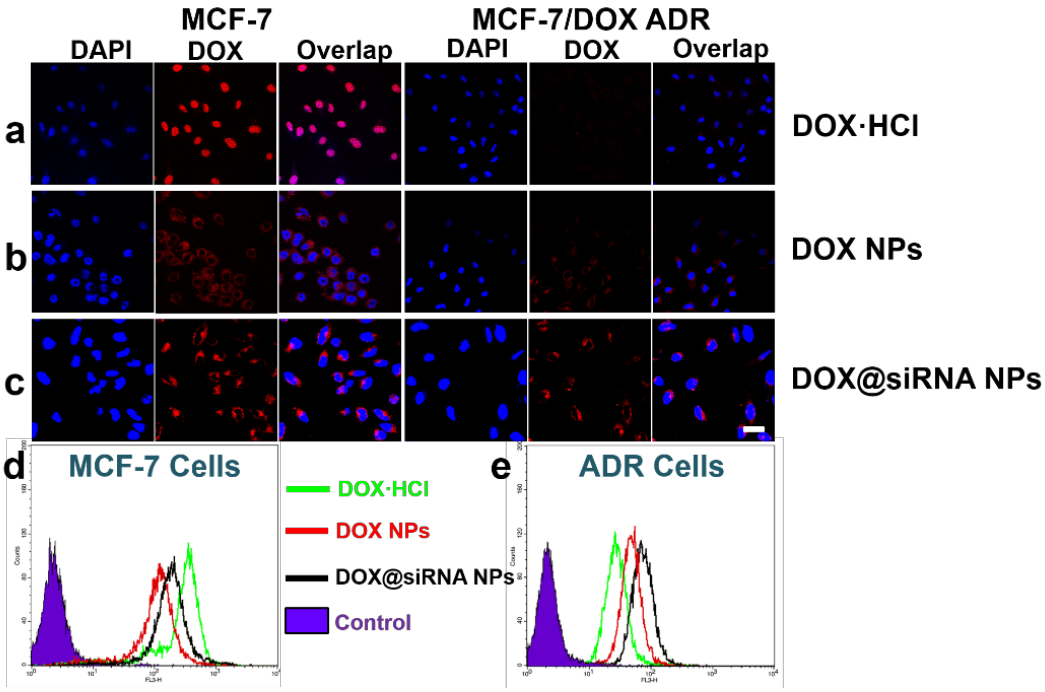

Figure 5. Cellular internalization of DOX@siRNA NPs in cancer cells. Subcellular localization of (a) DOX•HCl, (b) DOX NPs, (c) DOX@siRNA NPs in MCF-7 and MCF-7/DOX ADR cells after 4 h incubation. Blue and red indicates cell nuclei staining and DOX fluorescence, respectively. The flow cytometry analysis of the cellular internalization quantities of different drugs by (d) MCF-7 and (e) MCF-7/DOX ADR cells. Scale bar represents 20 μm.

Since DOX@siRNA NPs present a strong efficacy in killing both normal and drug resistant cancer cells, we next surveyed the cellular internalization ability of this material to obtain a basic understanding of their potency. In the initial experiment, the intracellular uptake of siRNA, DOX, and DOX@siRNA NPs by HeLa cells was studied by confocal microscopy as a test case. DOX has a red fluorescence, while siRNA was labeled with 6-carboxyfluorescein (FAM, green fluorescence) and nucleus was stained with 4′,6-diamidino-2-phenylindole (DAPI, blue fluorescence). DOX NPs and

lipofectamine 2000 carrying FAM-siRNA were used as two controls. As shown in Figure S3, after 4 h incubation, red fluorescence can be observed in the DOX NPs treated cells, and green fluorescence is detected in the lipo-siRNA treated cells. In the DOX@siRNA NPs group, both red fluorescence from DOX and green from FAM-labeled siRNA are able to be observed in cells, validating the contemporary cellular internalization of anticancer drugs and genes. This result demonstrates that simultaneous delivery of DOX and siRNA to cancer cells can be realized with our strategy, leading to the feasibility of producing cooperative effects.

After observing intracellular delivery of DOX@siRNA NPs in normal cancer cells, we also assessed their internalization in drug resistant ones. In the investigation, MCF-7 and MCF-7/ADR cells were incubated with DOX@siRNA NPs followed by confocal microscopy imaging (**Figure 5a-c**). DOX•HCl and DOX NPs were also studied for comparison. From these images, it can be seen that DOX•HCl can efficiently enter MCF-7 cells, but in a sharp contrast, the internalization of these molecules to MCF-7/ADR cells significantly drops. However, DOX@siRNA NPs treated MCF-7/ADR cells still display very strong red fluorescence. These findings are further supported by quantity analysis of the intracellular uptake by flow cytometry. **Figure 5d** indicates that DOX•HCl possess the highest intracellular uptake among the three groups when incubated with MCF-7 cells, but their internalization in MCF-7/ADR cells becomes the lowest. This observation can partially explain why DOX•HCl has very low efficacy in killing MCF-7/ADR cells although it works very well toward normal MCF-7 cells. In comparison, DOX@siRNA NPs incubated MCF-7/ADR cells present stronger

fluorescence than DOX•HCl and DOX NPs groups (**Figure 5e**). The mean values of DOX fluorescence within MCF-7/DOX ADR cells treated with DOX•HCl, DOX NPs and DOX@siRNA NPs are 29.49, 49.68 and 76.92, respectively (Table S1). The data are consistent with the observation from the confocal microscopy images, demonstrating that the DOX NPs coordinated with Bcl-2 siRNA can improve the therapeutics concentration in drug resistant cells. This is one of the reasons that DOX@siRNA NPs show the highest efficacy in killing MCF-7/ADR cells (**Figure 4**).

2.5. *In vivo* antitumor activity

We next explored their effectiveness in *in vivo* therapy. For this purpose, we firstly studied their pharmacokinetics in mouse model. BALB/c mice were treated with DOX@siRNA NPs, followed by analysis of the fluorescence of DOX in blood samples collected at different time points after injection. As shown in Figure S4, a long blood circulation half-life of 3.5 h is observed for DOX@siRNA NPs, whereas the circulation time of DOX•HCl is less than half of an hour. The prolonged circulation will increase drug delivery to tumors via enhanced permeability and retention (EPR) effect for high therapeutic efficacy.

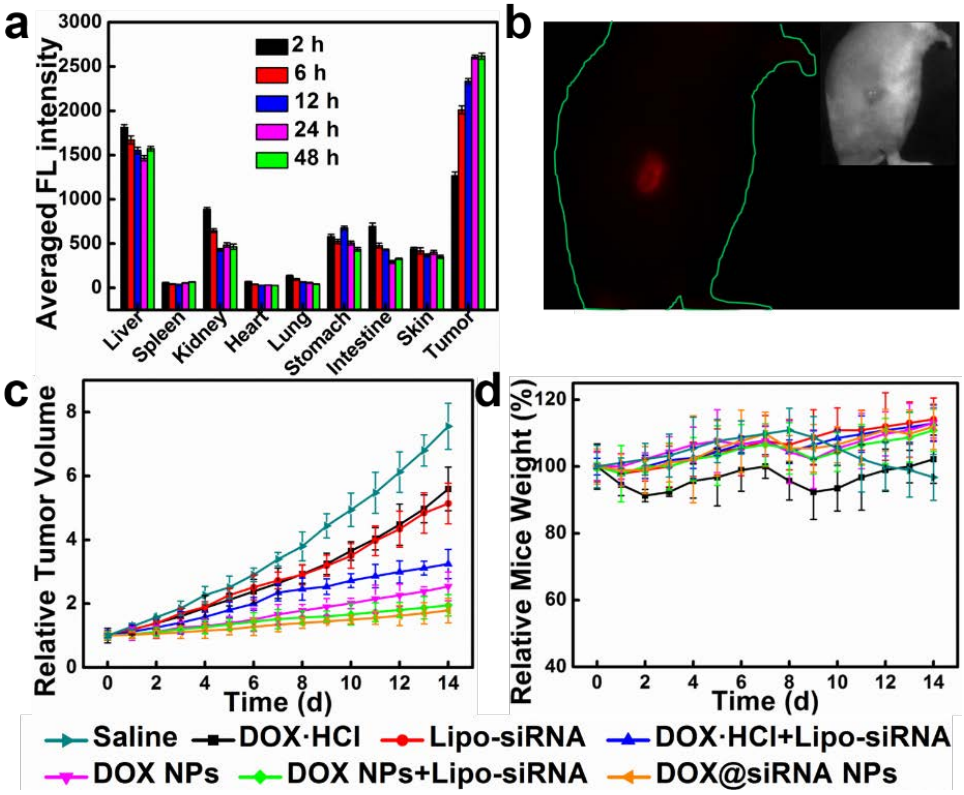

Figure 6. *In vivo* activities of DOX@siRNA NPs. (a) Biodistribution and (b) *in vivo* fluorescence image of DOX@siRNA NPs. (c) Evolution of the tumor volume after intravenous injection of (1) saline, (2) DOX•HCl, (3) Lipo-siRNA, (4) DOX•HCl plus Lipo-siRNA, (5) DOX NPs, (6) DOX NPs plus Lipo-siRNA, and (7) DOX@siRNA NPs. The formulation concentration was (2) 1 mg/kg DOX, (3) 10 μg siRNA, (4) 0.5 mg/kg DOX/5 μg siRNA, (5) 1 mg/kg DOX, (6) 0.5 mg/kg DOX/5 μg siRNA, and (7) 0.5 mg/kg DOX/5 μg siRNA. (d) Change of the body weight of 4T1 tumor bearing mice over time.

Following the half-life investigation of DOX@siRNA NPs, their biodistribution in major organs and tumors were detected by determining the fluorescence of DOX in tumor-bearing BALB/c mice. The fluorescence intensity of DOX in each organ was calculated by deducting the autofluorescence of untreated mice. **Figure 6a** shows that

30.50% of the administered NPs does appears in liver, and 21.34% in tumor at 2 h after NP administration. Other NPs mainly distribute in kidney (14.93%), intestine (11.70%) and skin (7.39%). Attractively, it is noted that the fluorescence intensity of tumor enhances with time. At 12 h post injection, 26.12% and 39.28% of the NPs are in liver and tumor tissue, respectively. At 48 h, the fluorescence intensity in tumor continues to increase, indicating 44.08% of NPs in the tumor tissue, which is more than that in the major organs. The high delivery amount of DOX@siRNA NPs can be attributed to the prolonged blood circulation time and the surface modification of NPs by PEG, which reduces the capture of NPs by the reticulo-endothelial (RES) system and correspondingly boosts drug accumulation in tumor.

To visibly observe the accumulation of nanomedicine in tumor, DOX@siRNA NPs were intravenously administered into BALB/c mice planted with 4T1 tumor followed by fluorescence imaging. It can be seen in **Figure 6b** that DOX@siRNA NPs treated mouse exhibits obvious red fluorescence in the tumor site at 6 h after injection. This result demonstrates the good potential of using these DOX@siRNA NPs for tumor imaging.

After we demonstrate that DOX@siRNA NPs have long half-life in blood circulation and can efficiently transport to tumor, the key issue will be whether this nanomedicine is able to effectively inhibit tumor growth with a low side effect. In the study, mice bearing 4T1 tumor were selected as animal models. When the tumor's sizes increased to 50-100 mm^3, the mice were randomly divided into several groups for testing the therapeutic function of DOX•HCl, Lipo-siRNA, DOX•HCl plus Lipo-

siRNA, DOX NPs, DOX NPs plus Lipo-siRNA, and DOX@siRNA NPs. The injection of drugs was administered twice on Day 0 and 7. Mice with injection of saline were applied as a negative control group.

During the therapy, the tumor volume and body weight of each mouse were monitored daily for 14 days. As displayed in **Figure 6c** and Figure S5, the tumor volume of saline treated group rapidly increases to 7.56±0.72 fold of the original value by the 14th day. The treatment of tumor by DOX•HCl and Lipo-siRNA can moderately slow down the tumor growth. Within the same time window, the tumor grows to 5.59±0.68 and 5.14±0.63 fold of the initial volume for DOX•HCl and Lipo-siRNA treated groups, respectively. Once DOX is made into the form of nanomedicine, the tumor inhibition efficacy dramatically improves. This is indicated by the much slower tumor growth to 2.54±0.45 fold of the starting volume. This can be partly ascribed to the extended blood circulation time of DOX NPs and the EPR effect of nanomedicine during *in vivo* application.[36,37] Similar to the findings from the *in vitro* test of cell anti-proliferative effect, the physical mixture of DOX NPs plus Lipo-siRNA can actually work substantially better than individual DOX NPs and Lipo-siRNA, which is proved by the tumor growth of only 1.95±0.33 fold. Most importantly, DOX@siRNA NPs group reveals the highest tumor inhibition ability (1.79±0.39 fold tumor growth) among all groups, thus confirming the *in vivo* synergistic therapeutic effect of DOX and Bcl-2 siRNA. We further carried out hematoxylin-eosin (H&E) and terminal deoxynucleotidyl transferase (TdT)-mediated dUTP nick-end labeling (TUNEL) assay staining of the tumor tissue of the treated mice. Compared with individual drugs,

DOX@siRNA NPs lead to obvious cell destruction, including lower nuclear-to-cytoplasmic ratio (H&E stain) and larger number of TUNEL-positive cells (Figure S6), providing a potentially synergistic antitumor efficacy for cancer therapy.

Although the tumor grow inhibition is just moderately better than the physical mixture of DOX-PEG NPs and Bcl-2 siRNA, we foresee that the tight binding of siRNA to the DOX NP surface will lead to less side effect. The reason is that siRNA can be better delivered to tumor together with DOX-PEG NPs. It can also avoid the possible widespread delivery of siRNA to healthy organs and tissues in its free molecule state.[38,39] To preliminarily investigate the safety performance of DOX@siRNA NPs, the body weights of all the above groups of mice were measured in **Figure 6d**. It is evident that the body weights of the mice treated with saline sharply drop after Day 8, which might be on accounts of excessive tumor growth. In comparison, the DOX@siRNA NPs treated mice do not show any sign of body weight reduction. These results prove that DOX@siRNA NPs at the used dose probably possess very low *in vivo* toxicity. Furthermore, the H&E staining of the major organs (heart, liver, spleen, lung, and kidney) of DOX@siRNA NPs treated mice (Figure S7) indicates that there are no noticeable organ damage and inflammatory lesion.

Bcl-2 siRNA has been tested in clinical trials; however, the anticancer effect of siRNAs is limited by many barriers, such as rapid degradation, less cellular uptake and poor tumor accumulation.[40,41] In this work, DOX@siRNA NPs possess enhanced stability in the physiological environment and prolonged blood circulation time (3.5 h) than Lipo-Bcl-2 siRNA, which is in use for clinical applications. Additionally, several

nanocarriers-based systems were previously reported for co-delivery of doxorubicin and Bcl-2 siRNA, but their drug loading capacity (DLC) is always low, such as glycol chitosan-based nanoparticles, cationic star-block terpolymer, mesoporous silica nanoparticles with DLC of approximately 10%, 20%, and 40%, respectively.[42,43,44] In significant contrast, the DLC of our DOX@siRNA NPs is as high as 87.18%, which is a step improvement. Beyond the high DLC, siRNA is plays a therapeutic role in the system, which means that the overall therapeutic component is even higher and we use negligible excipients. Overall, we designed an effective and safe strategy to deliver DOX and Bcl-2 siRNA for cancer therapy.

3. Conclusions

In conclusion, we put forward a novel strategy of using pure drug molecules to make nanoparticles for delivering siRNA and realizing synergistic anticancer therapy. As a test case, we synthesized DOX@siRNA NPs that are spherical and possess a diameter of about 55 nm. These NPs have significantly extended blood circulation half-life and can effectively enter DOX resistant MCF-7 cancer cells. In line with these characteristics, DOX@siRNA NPs result in stronger anti-proliferative effect than DOX•HCl, Lipo-siRNA and DOX NPs in drug resistant cancer cells, exhibiting synergistic anticancer efficacy. Most notably, DOX@siRNA NPs considerably inhibit tumor growth and exhibit very low toxicity. Overall, our method is able to achieve potent anticancer efficacy in tumor treatment and overcome drug resistance. We expect that this approach possesses significant potential for clinic applications.

4. Experiments

4.1. Preparation of DOX@siRNA NPs

To achieve DOX NPs, the hydrophilic DOX•HCl (99%, Beijing ZhongShuo Pharmaceutical Technology Development Co., Ltd.) was first converted to hydrophobic DOX, followed by addition of TEA at room temperature. The volume ratio of DOX•HCl/DMSO solution (1 mg/mL) to TEA is 10:1. Subsequently, 200 μL DOX/DMSO solution was dropwisely added into 10 mL water with active stirring, which generated DOX NPs in aqueous solution. C18PMH-PEG was prepared according to the previous report. In brief, 10 mg (1 eq) of C18PMH (Sigma, St. Louis, MO) and 143 mg (1 eq) of mPEG-NH_2 were dissolved in 5 mL of DCM reagent with the addition of 6mL of TEA and 11 mg of EDC. The reaction solution was under stirring for 24 h and then the DCM solvent was dried by nitrogen flow. The remained solid product was dissolved in water followed by 2 days of dialysis in water in a dialysis bag with an MWCO of 14 kDa to remove unreacted mPEG-NH_2. After lyophilization, the end product is a white solid which can be stored at 4℃. To modify the surface of as-prepared DOX NPs, 400 μL of 0.5 mg/mL C18PMH-PEG aqueous solution were added to 10 mL of DOX NPs solution followed by ultrasonic treatment of 5 min and room temperature incubation of 1 h. After this step, the DOX-PEG NPs were dropwisely added into PEI solution (1 mg/mL) and left for overnight to obtain DOX-PEG-PEI NPs. For siRNA loading, DOX-PEG-PEI NPs were diluted to different concentrations and added to the siRNA solution (20 mM) to obtain different N/P ratios in Mili-Q water/medium (Invitrogen, Carlsbad, USA). The tested N/P ratios include 0.5, 1, 2.5, 5, and 10. The drug loading efficiency of DOX was measured using HPLC (Agilent 1200).

Besides, the N/P ratio was calculated by the molar ratio of PEI nitrogen to RNA phosphate.

4.2.*In vitro* release profiles

The concentration of DOX@siRNA NPs was 0.5 μg/mL. In this experiment, siRNA was marked with fluorescein-labeled siRNA (FAM-siRNA, green fluorescence, Genpharm, Shanghai, China). DOX@siRNA NPs were placed into the release buffer, followed by immediate transformation to individual dialysis tubes with an MWCO of 14 kDa followed by immersion into 50 mL of buffers of different pH at 37 ℃. At different times, 2 mL of the buffer were removed from each group for fluorescence measurement and the same amount of fresh buffer was added. The released DOX and FAM-siRNA were determined by the fluorescence intensity. The released DOX and FAM-siRNA were quantified by measuring the fluorescence intensity. (DOX Ex/Em: 490/596 nm; FAM Ex/Em: 490/515 nm). These experiments were carried out in triplicate and the average values are shown.

4.3.Cell culture

A human cervical cell line (HeLa cells), murine 4T1 breast cancer cell line (4T1 cells), human breast adenocarcinoma cell line (MCF-7 cells) and DOX resistant derivatives of MCF-7 cells overexpressing Bcl-2 (MCF-7/ADR cells) were from American Type Culture Collection (ATCC, Manassas, VA, USA).

4.4.Intracellular uptake of DOX@siRNA NPs

HeLa cells were seeded on coverslips and left for 24 h. Subsequently,

DOX@siRNA NPs were added and incubated with the cells for 3 h. Before observation with confocal microscopy, the culture medium was removed and the cells were washed twice with cold PBS (pH 7.4, 0.01M) and fixed with 4% formaldehyde (Sigma-Aldrich, St. Louis, USA). Finally, the cells were studied using a Leica laser scanning confocal microscope.

4.5.*In vitro* anti-proliferative effect

One hundred μL of complete media with HeLa, MCF-7/ADR, MCF-7, and 4T1 cells were seeded in 96-well plates (~6,000 cells/well) and incubated for 24 h. Subsequently, 25 μL of samples were placed to each well for incubation with the cells (37 ℃, 5% CO_2). After the cells were further incubated for 48 and 72 h, the cell viabilities were quantified with a standard MTT assay. CI is defined as: $CI = D_1/D_{m1} + D_2/D_{m2}$, D_1 and D_2 represent the concentrations of drug 1 and drug 2, respectively, that are combined to achieve a certain cytotoxicity, while D_{m1} and D_{m2} are the concentrations of the two individual drugs to generate the same antitumor effect.

4.6.Intracellular uptake by MCF-7 and DOX resistant MCF-7 cells

Normal MCF-7 cells and MCF-7/ADR cells were separately seeded into 24-well plates at a density of 5×10^4/well in DMEM medium containing 10% FBS for 18 h. The medium was then replaced by 1 mL of DMEM (serum free), DOX•HCl, DOX NPs, and DOX@siRNA NPs and incubated for 4 h with a DOX concentration of 20 μg/mL. After the incubation, the medium was removed and the cells were washed three times in PBS. The supernatant of centrifuge product was removed and the precipitate cells were

washed three times with PBS. Finally, the internalization of DOX in cells was observed by confocal microscopy. In addition to the confocal microscopy study, another batch of cells with the same treatment was washed, trypsinized, and collected for flow cytometric analysis.

4.7.Measurement of blood circulation half-life

All experiments involving animals were performed in accordance with the guidelines of the Institutional Animal Care and Use Committee. BALB/c mice were administered through intravenous injection of 200 μL of DOX@siRNA NPs and DOX·HCl containing the same DOX concentration of 1 mg/mL. At each time point, blood samples were collected and solubilized in lysis buffer for fluorescence intensity measurement.

4.10. Biodistribution

4T1 bearing BALB/c mice were treated with 200 μL of 1 mg/ml of DOX@siRNA NPs, followed by sacrifice at different time points. The fluorescence intensities of organs and tissues were measured. The tissue autofluorescence was subtracted to calculate the amount of DOX.

4.11. *In vivo* imaging

The hair of 4T1 tumor-bearing mice was removed followed by intravenous injection of 200 μL of DOX@siRNA NPs (DOX concentration was 1 mg/mL). An untreated mouse was used as a control. The DOX@siRNA NPs treated mice were imaged with a Maestro *in vivo* fluorescence imaging system (CRi Inc.) at 6 h post

injection.

4.12. *In vivo* antitumor activity

The mice were randomly split to 7 groups after the sizes of tumors were in the range of about 55-95 mm^3. Samples was injected into each group of mice via the tail vein. The treatment was repeated on day 7. The tumor size and body weight of each mouse were measured and recorded every day for an overall period of two weeks.

4.13. Tissue section analysis

4T1 tumor-bearing mice were euthanized at 14 days post administration with DOX@siRNA NPs. Subsequently, the organs (heart, liver, spleen, lung, and kidney) and tumors were dissected and fixed with 10% neutral buffered formalin and then embedded in paraffin. Afterwards, paraffin was sectioned into slices with a thickness of 4 μm for H&E staining and TUNEL assay. The mouse injected with saline was used as a control group.

Associated Content

Supporting Information

SEM images of DOX-PEG NPs and DOX-PEG-PEI NPs during the layer-by-layer self-assembly process. Combination index of DOX@siRNA NPs. Subcellular localization of DOX·HCl, DOX NPs and DOX@siRNA NPs in Hela cells after 4 h incubation. DOX fluorescence values measured in MCF-7 cells and MCF-7/DOX ADR cells with DOX·HCl, DOX NPs and DOX@siRNA NPs estimated by flow cytometry. The concentration of DOX·HCl and DOX@siRNA NPs in blood at different time points

after injection. The digital pictures of the tumors of mice before (Day 0) and after (Day 14) intravenous injection of different materials. Histological photomicrographs of H&E and TUNEL staining of the tumor sections of different groups with various treatments. H&E staining of the major organs (heart, liver, spleen, lung, and kidney) of DOX@siRNA NPs and saline treated mice.

Author Information

Corresponding Author

(X. J. Z.) Tel: +86-512-65880955 Email: xjzhang@suda.edu.cn;

(X. C.) Tel: +44(0)1316502784 Email: xianfeng.chen@oxon.org (Michael.Chen@ed.ac.uk);

(X. H. Z.) Tel: +86-512-65882631 Email: xiaohong_zhang@suda.edu.cn.

Notes

The authors declare no competing financial interest.

Acknowledgment

This work was supported by the National Natural Science Foundation of China (Grant Nos. 51672180, 51622306, and 21673151), Qing Lan Project, 111 project, and the Priority Academic Program Development of Jiangsu Higher Education Institutions (PAPD).

References

(1) Patel, N. R.; Pattni, B. S.; Abouzeid, A. H.; Torchilin, V. P. Nanopreparations to Overcome Multidrug Resistance in Cancer. *Adv. Drug Deliver. Rev.* **2013**, 65, 1748-

1762.

(2) Kunjachan, S.; Rychlik, B.; Storm, G.; Kiessling, F.; Lammers, T. Multidrug Resistance: Physiological Principles and Nanomedical Solutions. *Adv. Drug Deliver. Rev.* **2013**, 65, 1852-1865.

(3) Banzhaf, C. A.; Thaysen-Petersen, D.; Bay, C.; Philipsen, P. A.; Mogensen, M.; Prow, T.; Haedersdal, M. Fractional Laser-Assisted Drug Uptake: Impact of Time-related Topical Application to Achieve Enhanced Delivery. *Laser. Surg. Med.* **2017**, 49, 348-354.

(4) Cox, G.; Wright, G. D. Intrinsic Antibiotic Resistance: Mechanisms, Origins, Challenges and Solutions. *Int. J. Med. Microbiol.* **2013**, 303, 287-292.

(5) Li, J.; Green, A. A.; Yan, H.; Fan, C. H. Engineering Nucleic Acid Structures for Programmable Molecular Circuitry and Intracellular Biocomputation. *Nat. Chem*. **2017**, 9, 1056-1067.

(6) Mitter, N.; Worrall, E. A.; Robinson, K. E.; Li, P.; Jain, R.G.; Taochy, C.; Fletcher, S. J.; Carroll, B. J.; Lu, G. Q.; Xu, Z. P. Clay Nanosheets for Topical Delivery of RNAi for Sustained Protection against Plant Viruses. *Nat. Plants* **2017**, 3, 16207.

(7) Serasinghe, M. N.; Missert, D. J.; Asciolla, J. J.; Podgrabinska, S.; Wieder, S. Y.; Izadmehr, S.; Belbin, G.; Skobe, M.; Chipuk, J. E. Anti-Apoptotic BCL-2 Proteins Govern Cellular Outcome Following B-RAFV600E Inhibition and Can Be Targeted to Reduce Resistance. *Oncogene* **2015**, 34, 857-867.

(8) Chen, H.-C.; Kanai, M.; Inoue-Yamauchi, A.; Tu, H.-C.; Huang, Y.; Ren, D.; Kim, H.; Takeda, S.; Reyna, D. E.; Chan, P. M.; Ganesan, Y. T.; Liao, C.-P.; Gavathiotis, E.;

Hsieh, J. J.; Cheng, E. H. An Interconnected Hierarchical Model of Cell Death Regulation by the BCL-2 Family. *Nat. Cell Biol.* **2015**, 17, 1270-1281.

(9) Kanasty, R.; Dorkin, J. R.; Vegas, A.; Anderson, D. Delivery Materials for siRNA Therapeutics. *Nat. Mater.* **2013**, 12, 967-977.

(10) Benjaminsen, R. V.; Mattebjerg, M. A.; Henriksen, J. R.; Moghimi, S. M.; Andresen, T. L. The Possible "Proton Sponge" Effect of Polyethylenimine (PEI) Does Not Include Change in Lysosomal pH. *Mol. Ther.* **2013**, 21, 149-157.

(11) Zeng, Q.; Wen, H.; Wen, Q.; Chen, X.; Wang, Y.; Xuan, W.; Liang, J.; Wan, S. Cucumber Mosaic Virus as Drug Delivery Vehicle for Doxorubicin. *Biomaterials* **2013**, 34, 4632-4642.

(12) Yan, L.; Zhang, J.; Lee, C. S.; Chen, X. Micro- and Nanotechnologies for Intracellular Delivery. *Small* **2014**, 10, 4487-4504.

(13) Tang, S.; Yin, Q.; Zhang, Z.; Gu, W.; Chen, L.; Yu, H.; Huang, Y.; Chen, X.; Xu, M.; Li, Y. Co-Delivery of Doxorubicin and RNA using PH-Sensitive Poly (β-Amino Ester) Nanoparticles for Reversal of Multidrug Resistance of Breast Cancer. *Biomaterials* **2015**, 35, 6047-6059.

(14) Liu, H.; Li, Y.; Mozhi, A.; Zhang, L.; Liu, Y.; Xu, X.; Xing, J.; Liang, X.; Ma, G.; Yang, J.; Zhang, X. SiRNA-Phospholipid Conjugates for Gene and Drug Delivery in Cancer Treatment. *Biomaterials* **2014**, 35, 6519-6533.

(15) Oberoi, H. S.; Nukolova, N. V.; Kabanov, A. V.; Bronich, T. K. Nanocarriers for Delivery of Platinum Anticancer Drugs. *Adv. Drug Deliver. Rev.* **2013**, 65, 1667-1685.

(16) Zhang, J. F.; Chen, W. C.; Chen, R.; Liu, X. K.; Xiong; Kershaw, S. V.; Rogach,

A. L.; Adachi, C.; Zhang, X. H.; Lee, C. S. Organic Nanostructures of Thermally Activated Delayed Fluorescent Emitters with Enhanced Intersystem Crossing as Novel Metal-Free Photosensitizers. *Chem. Commun.* **2016**, 52, 11744-11747.

(17) Divsalar, A.; Saboury, A. A.; Nabiuni, M.; Zare, Z.; Kefayati, M. E.; Seyedarabi, A. Characterization and Side Effect Analysis of a Newly Designed Nanoemulsion Targeting Human Serum Albumin for Drug Delivery. *Colloid. Surface. B.* **2012,** 98, 80-84.

(18) Steichen, S. D.; Caldorera-Moore, M.; Peppas, N. A. A Review of Current Nanoparticle and Targeting Moieties for the Delivery of Cancer Therapeutics. *Eur. J. Pharm. Sci.* **2013**, 48, 416-427.

(19) An, F. F.; Li, Y. N.; Zhang, J. F. Carrier-Free Photosensitizer Nanocrystal for Photodynamic Therapy. *Mater. Lett.***2014**, 122, 323-326.

(20) Zhang, J.; Li, Y.; An, F. F.; Zhang, X.; Chen, X.; Lee, C. S. Preparation and Size Control of Sub-100 nm Pure Nanodrugs. *Nano Lett.*2**015,** 15, 313-318.

(21) Yu, C.; Zhou, M.; Zhang, X.; Wei, W.; Chen, X.; Zhang, X. Smart Doxorubicin Nanoparticles with High Drug Payload for Enhanced Chemotherapy against Drug Resistance and Cancer Diagnosis. *Nanoscale* **2015**, 7, 5683.

(22) Zhang, J.; Liang, Y. C.; Lin, X.; Zhu, X.; Yan, L.; Li, S.; Yang, X.; Zhu, G.; Rogach, A. L.; Yu, P. K. N.; Shi, P.; Tu, L. C.; Chang, C. C.; Zhang, X.; Chen, X.; Zhang, W.; Lee, C. S. Self-Monitoring and Self-Delivery of Photosensitizer-Doped Nanoparticles for Highly Effective Combination Cancer Therapy *in Vitro* and *in Vivo*. *ACS Nano* **2015**, 9, 95-100.

(23) Song, X. R.; Wang, X.; Yu, S. X.; Cao, J.; Li, S. H.; Li, J.; Liu, G.; Yang, H. H.; Chen, X. Co9Se8 Nanoplates as a New Theranostic Platform for Photoacoustic/Magnetic Resonance Dual-Modal-Imaging-Guided Chemo-Photothermal Combination Therapy. *Adv. Mater.* **2015**, 27, 3285-3291.

(24) Liu, J.; Wang, C.; Wang, X.; Wang, X.; Cheng, L.; Li, Y.; Liu, Z. Mesoporous Silica Coated Single-Walled Carbon Nanotubes as a Multifunctional Light-Responsive Platform for Cancer Combination Therapy. *Adv. Funct. Mater.* **2015**, 25, 384-392.

(25) Zang, Y.; Wei, Y.; Shi, Y.; Chen, Q.; Xing, D. Chemo/Photoacoustic Dual Therapy with mRNA-Triggered DOX Release and Photoinduced Shockwave Based on a DNA-Gold Nanoplatform. *Small* **2016**, 12, 756-769.

(26) Kong, F.; Zhang, X.; Zhang, H.; Qu, X.; Chen, D.; Servos, M.; Makila, E.; Salonen, J.; Santos, H. A.; Hai, M.; Weitz, D. A. Inhibition of Multidrug Resistance of Cancer Cells by Co-Delivery of DNA Nanostructures and Drugs using Porous Silicon Nanoparticles@Giant Liposomes. *Adv. Funct. Mater.* **2015**, 25, 3330-3340.

(27) Moriwaki, K.; Bertin, J.; Gough, P. J.; Orlowski, G. M.; Chan, F. K. M. Differential Roles of RIPK1 and RIPK3 in TNF-Induced Necroptosis and Chemotherapeutic Agent-Induced Cell Death. *Cell Death. Dis.* **2015**, 6, 1636.

(28) Zaidi, A. H.; Raviprakash, N.; Mokhamatam, R. B.; Gupta, P.; Manna, S. K. Profilin Potentiates Chemotherapeutic Agents mediated Cell Death via Suppression of NF-κB and Upregulation of p53. *Apoptosis* **2016**, 21, 502-513.

(29) Holohan, C.; Van Schaeybroeck, S.; Longley, D. B.; Johnston, P. G. Cancer Drug Resistance: an Evolving Paradigm. *Nat. Rev. Cancer* **2013**, 13, 714-726.

(30) He, C.; Lu, K.; Liu, D.; Lin, W. Nanoscale Metal-Organic Frameworks for the Co-Delivery of Cisplatin and Pooled SiRNAs to Enhance Therapeutic Efficacy in Drug-Resistant Ovarian Cancer Cells. *J. Am. Chem. Soc.* **2014**, 136(14), 5181-5184.

(31) Zhang, J. F.; Li, S. L.; An, F. F.; Liu, J.; Jin, S. B.; Zhang, J. C.; Wang, P. C.; Zhang, X. H.; Lee, C. S.; Liang, X. J. Self-Carried Curcumin Nanoparticles for *in Vitro* and *in Vivo* Cancer Therapy with Real-Time Monitoring of Drug Release. *Nanoscale* **2015**, 7, 13503-13510

(32) Zhou, M.; Zhang, X.; Yang, Y.; Liu, Z.; Tian, B.; Jie, J.; Zhang, X. Carrier-Free Functionalized Multidrug Nanorods for Synergistic Cancer Therapy. *Biomaterials* **2013**, 34, 8960-8967.

(33) Ciardiello, F.; Caputo, R.; Borriello, G.; Bufalo, D. D.; Biroccio, A.; Zupi, G.; Bianco A. R.; Tortora, G. ZD1839 (IRESSA), An EGFR-Selective Tyrosine Kinase Inhibitor, Enhances Taxane Activity in Bcl-2 Overexpressing, Multidrug-Resistant MCF-7 ADR Human Breast Cancer Cells. *Int. J. Cancer* **2002**, 98, 463-469.

(34) Hu, C. M. J.; Zhang, L. Nanoparticle-Based Combination Therapy toward Overcoming Drug Resistance in Cancer. Biochem. Pharmacol. **2012**, 83, 1104-1111.

(35) Zhao, F.; Yin, H.; Li, J. Supramolecular Self-Assembly Forming a Multifunctional Synergistic System for Targeted Co-Delivery of Gene and Drug. *Biomaterials* **2014**, 35, 1050-1062.

(36) Li, L.; Chen, C.; Liu, H.; Fu, C.; Tan, L.; Wang, S.; Fu, S.; Liu, X.; Meng, X.; Liu, H. Multifunctional Carbon-Silica Nanocapsules with Gold Core for Synergistic Photothermal and Chemo-Cancer Therapy under the Guidance of Bimodal Imaging.

Adv. Funct. Mater. **2016**, 26, 4252-4261.

(37) Prabhakar, U.; Maeda, H.; Jain, R. K.; Sevick-Muraca, E. M.; Zamboni, W.; Farokhzad, O. C.; Barry, S. T.; Gabizon, A.; Grodzinski, P.; Blakey, D. C. Challenges and Key Considerations of the Enhanced Permeability and Retention Effect for Nanomedicine Drug Delivery in Oncology. *Cancer Res*. **2013**, 73, 2412.

(38) Williford, J.-M.; Wu, J.; Ren, Y.; Archang, M. M.; Leong, K. W.; Mao, H.-Q. Recent Advances in Nanoparticle-Mediated siRNA Delivery. *Annu. Rev. Biomed. Eng.* **2014**, 16, 347-370.

(39) Gottesman, M. M.; Lavi, O.; Hall, M. D.; Gillet, J.-P. Toward a Better Understanding of the Complexity of Cancer Drug Resistance. *Annu. Rev. Pharmacol.* **2016**, 56, 85-102.

(40) Ozcan, G.; Ozpolat, B.; Coleman, R. L.; Sood, A. K.; Lopez-Berestein, B. Preclinical and Clinical Development of SiRNA-Based Therapeutics. *Adv. Drug Deliver. Rev.* **2015**, 87, 108-119.

(41) Lindqvist, L. M.; Heinlein, M.; Huang, D. C. S.; Vaux, D. L. Prosurvival Bcl-2 Family Members Affect Autophagy Only Indirectly, by Inhibiting Bax and Bak. *PNAS.* **2014**, 111, 8512-8517.

(42) Yoon, H. Y.; Son, S.; Lee, S. J.; You, D. J.; Yhee, J. Y.; Park, J. H.; Swierczewska, M.; Lee, S.; Kwon, I. C.; Kim, S. H.; Kim, K.; Pomper, M.G. Glycol Chitosan Nanoparticles as Specialized Cancer Therapeutic Vehicles: Sequential Delivery of Doxorubicin and Bcl-2 SiRNA. *Sci. Rep.* **2014**, 4, 6878.

(43) Qian, J. M.; Xu, M. H.; Suo, A. L.; Xu, W. J.; Liu, T.; Liu, X. F.; Yao, Y.; Wang,

H. J. Folate-Decorated Hydrophilic Three-Arm Star-Block Terpolymer as a Novel Nanovehicle for Targeted Co-Delivery of Doxorubicin and Bcl-2 siRNA in Breast Cancer Therapy. *Acta Biomater.* **2015**, 15, 102-116.

(44) Chen, A. M.; Zhang, M.; Wei, D. G.; Stueber, D.; Taratula, O.; Minko, T.; He H. X. Co-Delivery of Doxorubicin and Bcl−2 siRNA by Mesoporous Silica Nanoparticles Enhances the Efficacy of Chemotherapy in Multidrug-Resistant Cancer Cells. *Small* **2009**, 5, 2673-2677.

Table of Contents Image

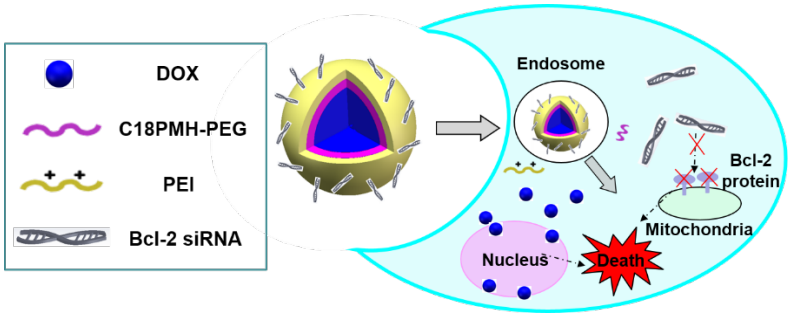

Supporting Information

Doxorubicin@Bcl-2 siRNA core@shell nanoparticles for synergistic anticancer chemotherapy

Mengjiao Zhou,[+] Xiujuan Zhang,[+,] Xiuzhen Xu,[+] Xianfeng Chen,[‡,*] and Xiaohong Zhang[+,*]*

+Jiangsu Key Laboratory for Carbon-Based Functional Materials & Devices, Institute of Functional Nano & Soft Materials (FUNSOM), Joint International Research Laboratory of Carbon-Based Functional Materials and Devices, Soochow University, 199 Ren'ai Road, Suzhou, 215123, Jiangsu, PR China.

‡School of Engineering, Institute for Bioengineering, The University of Edinburgh, King's Buildings, Mayfield Road, Edinburgh EH9 3JL, United Kingdom.

Corresponding Author

(X. J. Z.) Tel: +86-512-65880955 Email: xjzhang@suda.edu.cn;

(X. C.) Tel: +44(0)1316502784 Email: xianfeng.chen@oxon.org (Michael.Chen@ed.ac.uk);

(X. H. Z.) Tel: +86-512-65882631 Email: xiaohong_zhang@suda.edu.cn.

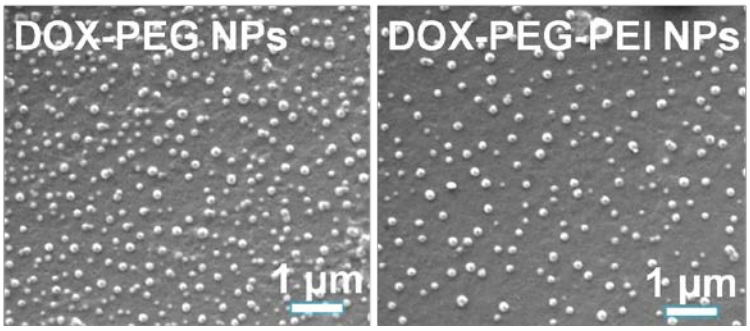

Figure S1. SEM images of DOX-PEG NPs and DOX-PEG-PEI NPs during the layer-by-layer self-assembly process.

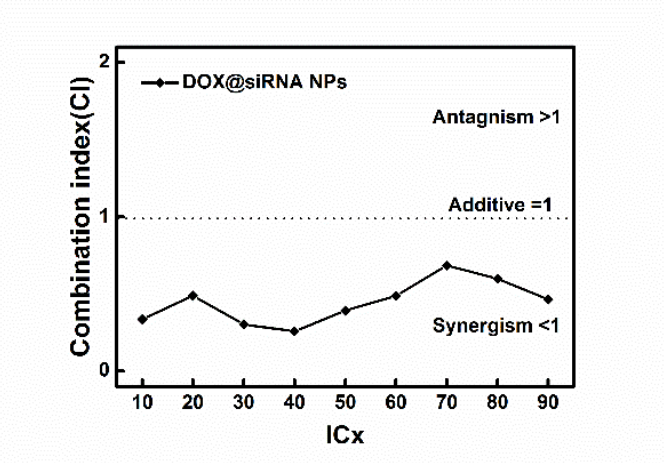

Figure S2. Combination index of DOX@siRNA NPs against HeLa cells.

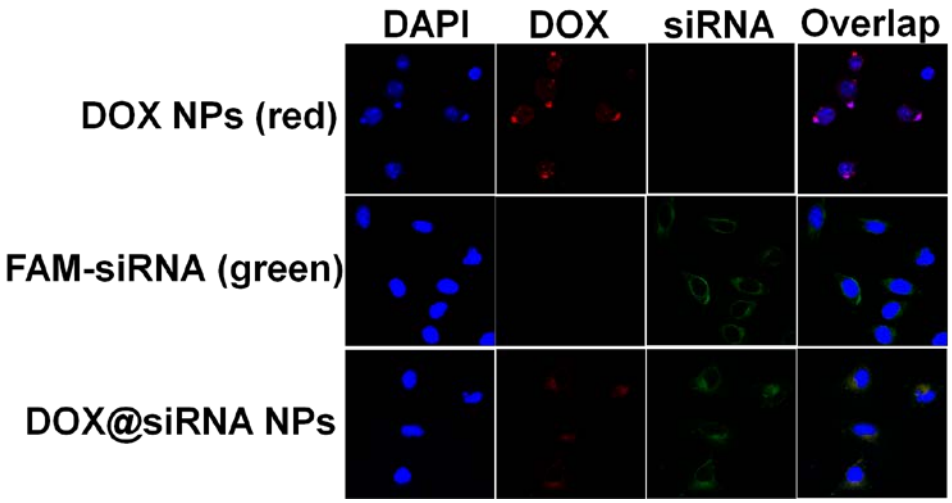

Figure S3. Subcellular localization of DOX·HCl, DOX NPs and DOX@siRNA NPs in Hela cells after 4 h incubation. Blue represents the fluorescence of DAPI for cell nuclei staining, red indicates the fluorescence of DOX for monitoring drug delivery, green indicates the fluorescence of fluorescein-labeled siRNA (FAM-siRNA).

	DOX HCl	DOX NPs	DOX@siRNA NPs
MCF-7 Cells	311.11	124.35	208.49
MCF-7 ADR Cells	29.49	49.68	76.92

Table S1. DOX fluorescence values measured in MCF-7 cells and MCF-7/DOX ADR cells with DOX·HCl, DOX NPs and DOX@siRNA NPs estimated by flow cytometry.

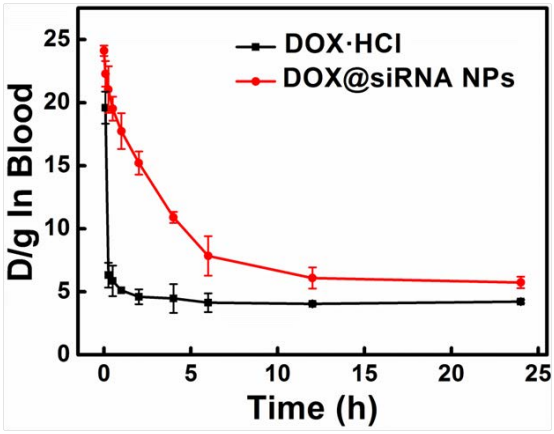

Figure S4. The concentration of DOX·HCl and DOX@siRNA NPs in blood at different time points after injection. The unit was the percentage of injected dose per gram tissue (% ID g^{-1}).

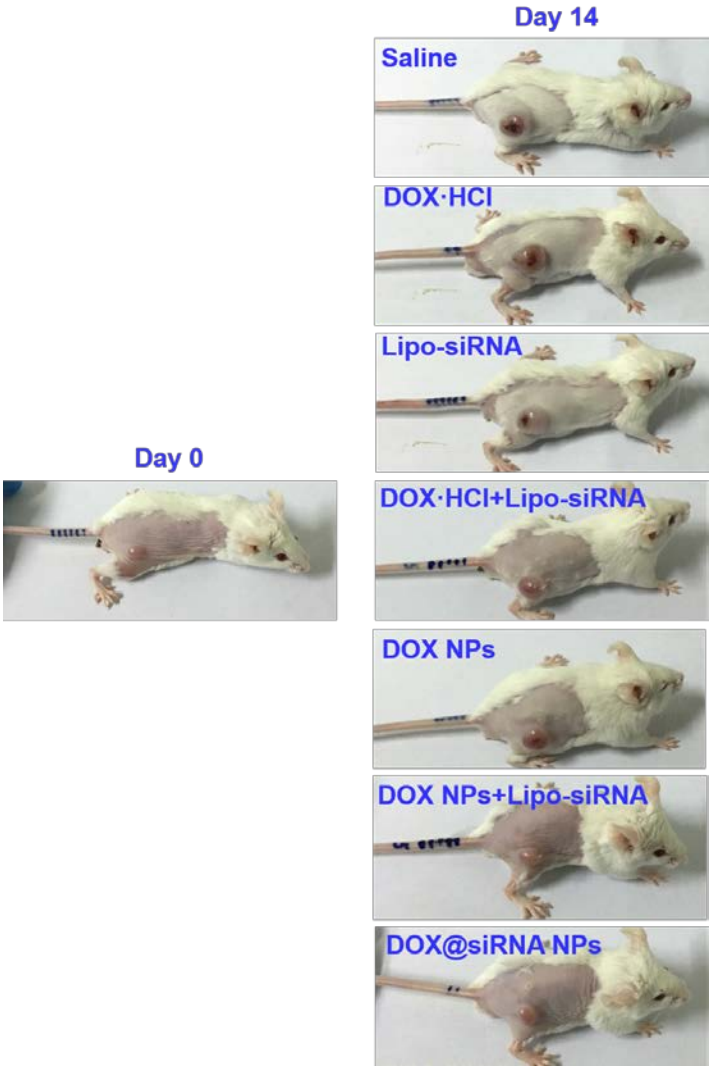

Figure S5. The cameral images of mice tumors after intravenous injection of different groups at Day 14, the cameral image of Day 0 was set as control.

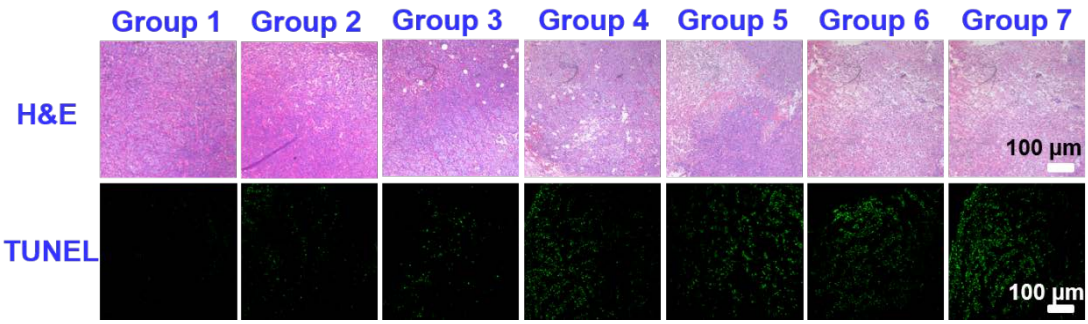

Figure S6. Histological photomicrographs of H&E and TUNEL staining of the tumor sections of different groups with various treatments, including (1) saline, (2) DOX•HCl, (3) Lipo-siRNA, (4) DOX•HCl plus Lipo-siRNA, (5) DOX NPs, (6) DOX NPs plus Lipo-siRNA, and (7) DOX@siRNA NPs. The formulation contained (2) 1 mg/kg DOX, (3) 10 μg siRNA, (4) 0.5 mg/kg DOX/5 μg siRNA, (5) 1 mg/kg DOX, (6) 0.5 mg/kg DOX/5 μg siRNA, and (7) 0.5 mg/kg DOX/5 μg siRNA.

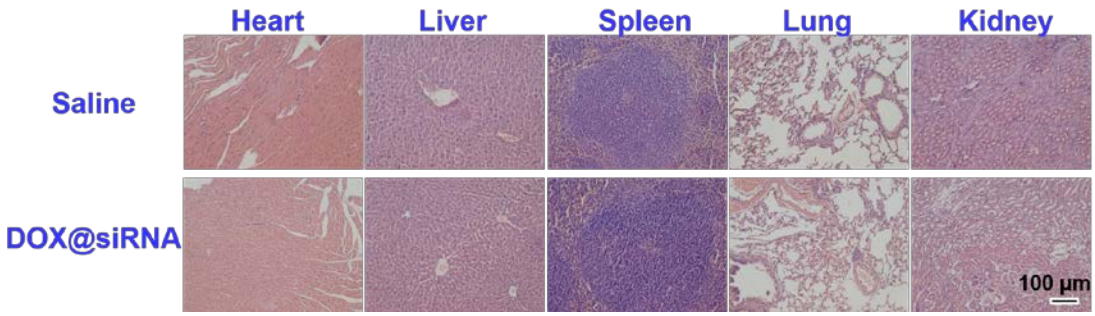

Figure S7. H&E staining of the major organs (heart, liver, spleen, lung, and kidney) of DOX@siRNA NPs and saline treated mice (organs collected at 14 days after initial treatment) (100× magnification).